ANALYTICAL EVALUATION OF CYCLIC LOADING BEHAVIOR OF CIRCULAR STEEL COLUMNS RETROFITTED BY EXTERNALLY BONDED CARBON FIBER SHEETS IN GRADED CONFIGURATION

Tokyo Metropolitan University Student Member ○Juliane Therese R. Bacod
Tokyo Metropolitan University Regular Member Hitoshi Nakamura
Toray Industries, Inc. Regular Member Takahiro Matsui

1. INTRODUCTION

Circular steel columns, commonly used as bridge piers due to its applicability to narrow sites and high strength capacity, are identified to be susceptible to local buckling when subjected to strong lateral loads. Carbon fiber (CF) sheet wrapping is one of the well-known seismic retrofitting techniques used to address this. Despite of the many advantages of this method, existing studies show that it still results to diamond buckling that causes sudden decrease in the load-carrying capacity upon failure.

In this study, experimental and analytical evaluation of the reinforcement and repair effect of carbon fiber sheets arranged in graded configuration to circular steel columns were conducted. Analytical results from the implemented finite element analysis (FEA) models were verified using the experimental results from the cyclic loading test conducted in a previous study.

2. SPECIMEN DESIGN AND EXPERIMENTAL SET-UP

2.1 Circular Steel Column

The specimen in this study is a hollow circular steel column (JIS STK400) as shown in **Fig. 1**. Material properties of the steel are presented in **Table 1**. Stiffening ribs and a thicker section were incorporated to the specimen to prevent buckling near the base of the column. The specimen is anchored to the ground using 12 – M36 bolts tightened by hydraulic bolt tensioning.

2.2 CF Sheet Reinforcement

Two CF sheet reinforcement cases were considered: 1) the application of CF sheets on column specimen before loading (reinforcement model, R) and 2) application of CF sheets after the column specimen have undergone failure (repair model, S). Both cases utilize the 10-4/150-250 graded configuration shown in **Fig. 2(a).** Note that the unreinforced (N) specimen serves as the benchmark and control set up at which results from the reinforcement and repair cases were evaluated.

The properties of the resulting CF reinforced polymer (CFRP) are calculated using Halpin-Tsai approximate equations – with consideration of the upper and lower bound CFRP elastic moduli. Material properties of the CF sheet, epoxy resin, and CFRP are summarized in **Table 1**.

2.3 Loading Program

The specimen was subjected to a constant axial load to represent the superstructure weight – 10% of the yielding axial force (492.9kN). An increasing cyclic lateral load was applied at the top of the specimen by displacement control as shown in the loading program in **Fig. 2(b)** and **(c).** The loading program is composed of increasing increments of the calculated horizontal yield displacement (δ_y) of the column. The dimensions of the specimen, loading program, and CF sheet reinforcement cases were adopted from an existing study (Magtagñob et.al, 2021).

3. FINITE ELEMENT MODEL

3.1 Modeling of Column Specimen

Finite element analysis was performed using large strain nonlinear updated Lagrange procedure of the general-purpose finite element program MSC Marc/Mentat 2019. Models considered in the FEA are summarized in **Table 2.** Steel elements were modeled using 4-node thick shell elements while the CFRP was modeled using 4-node thin shell elements. Lower regions of the model up to 300 mm above the reinforcement area were modeled using 10 x 20 mm mesh size to accurately capture buckling deformations and stress concentrations. The steel was modeled using elasto-plastic material with Hill yield criterion and kinematic hardening

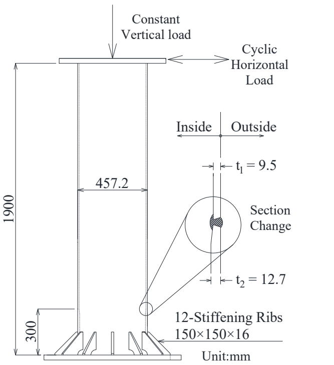

Fig. 1 Schematic diagram of test specimen

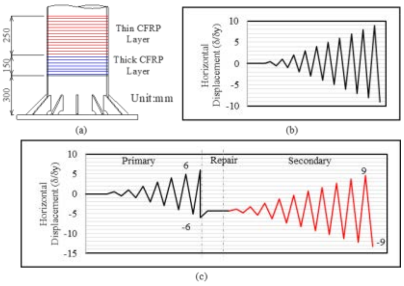

Fig. 2 Reinforcement Diagram and Loading Program
(a) Graded Reinforcement Configuration (b) Reinforcement Specimen Loading, (c) Repair Specimen Loading

Table 1 Material Properties

Material	Properties	Symbols	Values	Units
Steel (JIS STK400)	Elastic modulus	E	190,200	MPa
	Yield stress	σ_y	363	MPa
Carbon Fiber Sheet (UT70-30G)	Elastic modulus (0˚)	E_{cfl}	245,000	MPa
	Poisson's ratio (0˚)	ν_{cfl}	0.2	-
	Design thickness	t_{cf}	0.167	mm
Epoxy Resin (AUP40)	Elastic modulus	E_m	3,430	MPa
	Poisson's ratio	ν_m	0.39	-
CFRP	Fiber content	V_f	50	%
	Thickness (10-layer)	t_{cfrp}	0.334	mm
	Longitudinal Elastic modulus	E_1	111,800	MPa
		E_{1ub}	124,200	MPa
		E_{1lb}	6,800	MPa
	Transverse Elastic modulus	E_2	12,900	MPa
		E_{2ub}	7,800	MPa
		E_{2lb}	5,400	MPa
	Shear modulus	G_{12}	3,600	MPa
	Poisson's ratio	ν_{12}	0.29	-

Table 2 Summary of Models

Model	Classification	Hardening Law	CFRP Compression Resistance
N-0	No Reinforcement	Kinematic, f_h = 1.0	-
N-1	No Reinforcement	Combined, f_h = 0.85	-
R-0C	Reinforcement	Kinematic	Compression Resistant
R-0NC	Reinforcement	Kinematic	Non-compression Resistant
S-0C	Repair	Kinematic	Compression Resistant
S-0NC	Repair	Kinematic	Non-compression Resistant

Keywords: Carbon fiber sheet, Numerical simulation, Finite element analysis, Circular steel columns
Contact address: Minami-Osawa 1-1, Hachioji-shi, Tokyo, 192-0397, Japan, Tel: +81-42-677-1111, Ext. 4564

law of plasticity. The CFRP was modeled using orthotropic material with defined strain limits to account for the calculated tensile and compressive capacity of the CFRP. Steel and CFRP elements were bonded using the glued cohesive contact analysis option in MSC Marc/Mentat 2019 wherein the contact stiffness was defined by the properties of the AUP40 resin.
The base plate and 12 – M36 bolts were modeled to explicitly account for the specimen's base boundary condition as shown in **Fig. 3**. Overclosure tying constraints were used to simulate the bolt pretension force. Explicit modeling of base conditions simulates the potential occurrence of base displacements which affects the overall behavior of the specimen.

4. RESULTS AND DISCUSSION

4.1 Experimental Results

The unreinforced specimen (N-EXP) reached failure at $\pm 6\delta_y$ cycle at which an elephant foot buckling mode was observed. Summarized in **Table 3** are the experimental results for the reinforcement specimen (R-EXP) and repair specimen (S-EXP) in comparison with N-EXP.
R-EXP exhibited increase on both horizontal load capacity and ductility, thus, suppressing the buckling deformations which caused N-EXP failure at earlier loading cycles. Initial CFRP debonding/cracking was observed at $-6\delta_y$ upon reaching the maximum horizontal load. On the other hand, S-EXP exhibited recovery of the N-EXP horizontal capacity and ductility even after the specimen has undergone failure from primary loading.

4.2 Verification of Finite Element Model

Horizontal load and displacement capacity

Generally, considered FEA models were in good agreement with the experimental results. Summarized in **Table 4** are the calculated $\%_{error}$ for each model with respect to results of its corresponding experimental specimen. Also, shown in **Fig. 4 (a)** and **(b)** are the comparison of load-displacement envelope curves from experimental and analytical studies.
For the simulation of the unreinforced specimen, N-0 considered pure kinematic hardening for steel plasticity while N-1 considered combined hardening factor, f_h=0.85. As shown in **Fig. 4**, both models were able to approximate the initial rigidity and pre-yielding behavior of N-EXP. However, both models exhibited faster decrease in horizontal load capacity at the post-peak branch of the envelope curve. For R and S FEM, it was decided to maintain the N-0 model for the steel specimen.
For R- and S-FEM, two models were considered: 1) considering CFRP's compression resistance and 2) assuming CFRP has no compression resistance. For the reinforcement case, both R-0C and R-0NC are in good agreement with R-EXP up to $\pm 6\delta_y$ cycle which correspond to R-EXP's maximum horizontal load. R-0C better approximates R-EXP behavior up to $\pm 8\delta_y$ compared to R-0NC which has faster decrease in capacity after CFRP failure at $\pm 6\delta_y$. For the repair case, S-0C and S-0NC were subjected to a primary loading up to $\pm 5\delta_y$ since this point of the FEA generates the equivalent buckling deformation from N-EXP failure at $\pm 6\delta_y$. The positive loading behavior generated from S-0C and S-0NC models sufficiently approximates S-EXP specimen's behavior. However, only the rigidity and re-yielding after repair was capture for the negative loading side.

Buckling Deformation

Fig 5. shows the buckling deformation of N-0, R-0C, and S-0C at final loading. N-0 was able to capture the elephant foot buckling observed in the experiment. In R-0C model, stress concentration shifted on upper sections of the column reinforcement since an inward bulge was observed between h=450 to 500 mm where the thin CFRP layers are located. Lastly, in S-0C model, the tensile failure of the CFRP that occurred at the S-EXP specimen was captured by the outward buckling at the negative side of model.

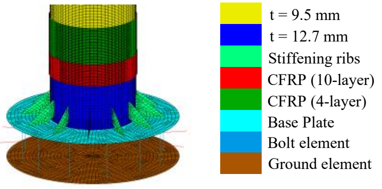

Fig 3 Finite Element Model

Table 3 Comparison of Experimental Results

Model	(+) direction		(-) direction	
Maximum Horizontal Load				
	H_{max} (kN)	% increase	H_{max} (kN)	% increase
N-EXP1	418.4	-	-417.3	-
R-EXP	479.5	13%	-462.0	10%
S-EXP	453.2	8%	-409.0	2%
Ductility				
	μ_{95}	% increase	μ_{95}	% increase
N-EXP1	6.0*	-	-5.1	-
R-EXP	8.1*	26%	-8.0*	36%
S-EXP	8.1*	25%	-5.5	8%

*Maximum load only dropped by less than 5% at last load increment

Table 4 Comparison of Experimental and Analytical Results

Model	(+) direction		(-) direction	
	H_{max} (kN)	$\%_{error}$	H_{max} (kN)	$\%_{error}$
N-0	406.1	2.9%	-406.3	2.6%
N-1	420.7	0.5%	-416.0	0.3%
R-0C	479.8	0.1%	-479.2	3.7%
R-0NC	468.3	2.3%	-461.8	0.04%
S-0C	472.9	4.3%	-402.1	1.7%
S-0NC	446.0	1.6%	-393.4	3.8%

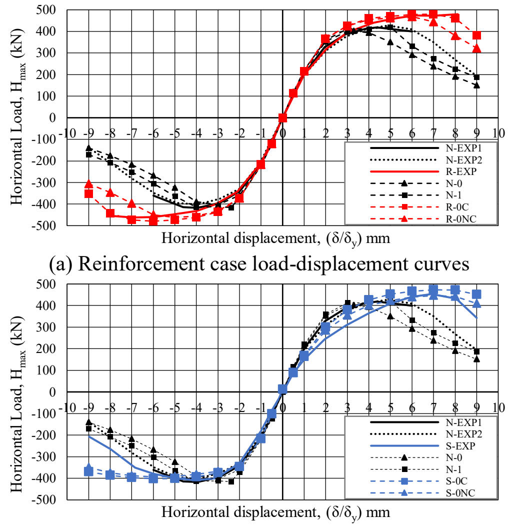

(a) Reinforcement case load-displacement curves

(b) Repair case load-displacement curves

Fig. 4 Comparison of Experimental and Analytical Results

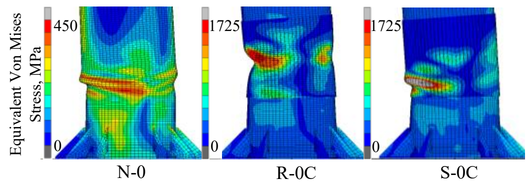

Fig. 5 Buckling deformations at final loading ($-9\delta_y$)

5. CONCLUSION

The results showed that the reinforcement model can slightly improve the horizontal load capacity and can effectively increase the ductility of the steel column. The repair model can sufficiently recover the column's horizontal load capacity and ductility. The implemented finite element analysis model can adequately evaluate the horizontal loading capacity and buckling modes of the reinforcement and repair models. Evaluation of other CF sheet configurations can be considered to eventually address the inward buckling deformations on the reinforcement model and to further delay the failure on repair models.

REFERENCES

Magtagñob, K., Nakamura, H., Matsui, T.,: Effect of Graded Carbon Fiber Sheet Configuration on the Seismic Retrofitting of Circular Steel Bridge Piers, *Proceedings of the 14th Symposium on Research and Application of Hybrid and Composite Structures*, pp.11-1-11-8, 2021.11